Appl Phys B (2011) 105:255–261
DOI 10.1007/s00340-011-4687-9

Applied Physics B
Lasers and Optics

Direct shaping of picosecond high energy deep ultraviolet pulses

A. Trisorio · C. Ruchert · C.P. Hauri

Received: 24 January 2011 / Revised version: 25 May 2011 / Published online: 20 August 2011

Abstract We demonstrate temporally shaped pulses in the deep ultraviolet spectral range (270 nm) with energies up to 37 μJ using an efficient prism stretcher and an acousto-optic programmable dispersive filter (AOPDF) applied directly in the UV. The scheme allows for arbitrary phase and amplitude shaping of picosecond UV pulses at high energy in a simple and efficient way.

1 Introduction

Modern Ti:sapphire lasers routinely permit the production of high energy femtosecond pulses in the UV by tripling the fundamental frequency in nonlinear crystals. Temporally shaped femtosecond UV laser pulses play an important role in the exploration of ultrafast phenomena in femtochemistry to control chemical reactions [1, 2] or to measure atomic quantum states [3], for example. Temporal shaping of high-energy UV pulses is equally important for modern large scale femtosecond x-ray sources like x-ray Free Electron Laser (FELs) and Energy Recovering Linacs (ERLs) [4, 5]. There UV laser pulses are typically used to produce electron bunches by the photoelectric effect on metallic surfaces or semiconductors which are subsequently accelerated in radiofrequency cavities up to several GeV. Indeed, the UV pulse temporal profile is directly correlated with the longitudinal electron bunch density. For FEL and ERLs, a homogeneous longitudinal electron density distribution is favorable since it minimizes nonlinear contributions of space charge forces within the bunch. Simulations indicate that a longitudinal flattop-like intensity profile with fast rising/falling edges and low modulations on the top is one of the most favorable shapes to maintain the high brilliance of the electron beam during transportation from the gun to the linear accelerator [4, 6, 7]. Typically, pulses of 3 to 10 ps in duration and several tens of μJ in energy are required to drive such photoelectron guns. A fully tailorable UV pulse source would allow for the generation of low emittance electron beams. This is a prerequisite for future compact FELs.

The generation of flattop-like or even arbitrarily shaped temporal pulses at high energy is, however, still challenging in the 250–300 nm spectral range. A direct transfer of well-established near-IR pulse shaping techniques [8] to the UV spectral region has turned out to be difficult. Conventional near-infrared liquid crystal modulators (LCMs), for example, suffer from strong absorption in the UV. Up to present, no commercial UV LCM has been available. However, promising results have very recently been obtained with a laboratory prototype [9]. In the past, the lack of LCM adapted to the 250–300 nm spectral range obliged researchers to explore *indirect* pulse shaping where the fundamental near-infrared pulse waveform was tailored prior to frequency conversion [10–12]. Even though this technique has proven some potential, it suffers from two main drawbacks. Firstly, cascaded nonlinear frequency conversion stages required for the generation of radiation with $\lambda < 300$ nm tend to modify the frequency-converted pulse shape. In fact, the nonlinear frequency conversion process enhances significantly temporal and spatial intensity modulations and may lead to pulse distortion. The UV temporal

A. Trisorio (✉) · C. Ruchert · C.P. Hauri
Paul Scherrer Institute, 5232 Villigen PSI, Switzerland
e-mail: alexandre.trisorio@psi.ch
Fax: +41-56-3104488

C.P. Hauri (✉)
Ecole Polytechnique Federale de Lausanne, 1015 Lausanne, Switzerland
e-mail: christoph.hauri@psi.ch
Fax: +41-56-3104488

pulse shape is thus not simply a frequency-shifted copy of the fundamental but undergoes nonlinear pulse distortions. A complex phase-and-amplitude feedback loop on the fundamental pulse shape is usually required to achieve a desired complex pulse shape in the UV. This often leads, secondly, to a fundamental pulse shape which is inappropriate for reaching highest IR-to-UV conversion efficiency.

Direct amplitude and phase shaping in the UV is intrinsically free of these drawbacks. A promising technique is based on an acousto-optic modulator (AOM) device situated in a $4f$ zero-dispersion optical beam line [13, 14]. The AOM offers spectral amplitude shaping capability and a high spectral resolution (typically 0.01 nm/mm aperture) [13, 15]. Another main advantage of this technique is that the fused silica AOM have a two-photon absorption coefficient [16] which is about one order of magnitude lower than the one of the UV AOPDF crystal ($\beta = 2.7\text{E-}10$ cm/W) used in our experiment [17]. However, this setup has a high alignment complexity. Another approach consists of the use of a micromirror array placed in a $4f$ zero-dispersion optical beam line [18, 19]. In addition to alignment complexity, the reported diffraction pattern in the beam (due to the segmented array) and the limited amount of spectral phase introduced by the device [20, 21] make it inappropriate for our application. Very recently, an acoustooptic programmable dispersive filter (AOPDF) for the UV has been presented for producing femtosecond pulse trains at 270 nm but at an energy level which is significantly below the requirements for FEL and ERL related applications [22–24].

In this paper, we present a direct UV temporal shaping technique for the generation of arbitrarily shaped picosecond (ps) pulses at the energy level required for FEL application. The scheme consists of a highly efficient UV fused silica prism stretcher and an AOPDF adapted to the UV spectral region [24] and allows temporal stretching of the initial 100 fs long UV pulses up to 10 ps. Amplitude and phase control directly in the UV enables the generation of shaped high-energy UV pulses without affecting the THG conversion efficiency. We demonstrate the powerful shaping capability of the scheme by generating a flattop pulse shape as well as a ramp-like and "M shaped" pulse forms and discuss furthermore its technical limitations. Our scheme offers an easy-to-align and tailorable picosecond UV laser source.

2 Experimental setup

The experimental setup is shown in Fig. 1. The Ti:Sa laser source delivers transform-limited 18 mJ, 50 fs pulses (FWHM) at a central wavelength of 810 nm and at a repetition rate of 100 Hz. Third harmonic (TH) radiation is generated via sum frequency mixing of the fundamental pulse with its second harmonic in a 200 µm thick BBO

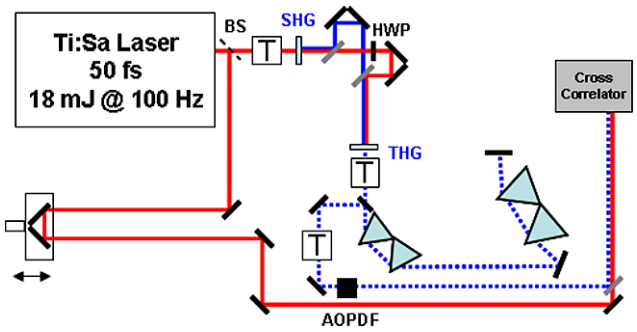

Fig. 1 Experimental setup for UV temporal pulse shaping. The fundamental beam is frequency tripled to generate 270.6 nm radiation. Femtosecond UV pulses are stretched in a UV-fused silica prism line and temporally shaped with the UV acoustooptic programmable dispersive filter (AOPDF). The pulses are temporally characterized with a commercial scanning cross-correlator apparatus. BS: beam splitter, T: telescope, SHG: 350 µm-type 1 BBO crystal, THG: 200 µm-type 1 BBO crystal

(β-barium borate, type I) crystal. The TH pulses have energies of up to 1 mJ at a wavelength of 270 nm with a Gaussian-like spectral shape (1.3 nm FWHM, Fig. 3b). This corresponds to transform limited pulse duration of 83 fs FWHM. The femtosecond UV pulses are subsequently stretched by double-passing a double-prism assembly. The prism substrate (Corning 7980 HPFS, grade AA) is a high purity synthetic amorphous silicon dioxide and has been carefully selected due to its exceptional transmittance properties in the deep ultraviolet (T internal >99.85%/cm for 270 nm). To avoid nonlinear absorption in the prism substrate, the beam diameter is expanded to a diameter of 40 mm prior to the stretcher. The maximum intensity at the first prism face is around 800 MW cm^{-2}, and thus well below the limit for two-photon absorption (>1 GW cm^{-2}) [25]. The setup allows easy pulse stretching up to 10 ps by simply changing the prisms separation (≈3 ps/meter). The optical face dimensions of the prisms are L ∗ H = 100 mm ∗ 150 mm. The maximum distance between the two prism pairs is 3.5 m. Larger separation results in an overfilling of the third prism entrance face by the dispersed beam. The overall transmission of the prism stretcher is measured to be ≈85% (including losses from two retroreflector mirrors) which is significantly higher than for an equivalent grating-based UV stretcher (typically 25%). After the stretcher, the beam is sent toward the UV AOPDF (DAZZLER^{TM} model T-UV 250–400 from Fastlite). A telescope prior to the AOPDF adjusts the transverse beam size to the nominally accepted beam size of this device (1.5 mm diameter). For temporal pulse characterization a commercial scanning difference frequency mixing (DFM) cross-correlator is used in a noncollinear geometry (PulseCheck, APE GmbH). A beam splitter ($R = 0.5\%$) located after the Ti:sapphire compressor provides the fundamental 50 fs probe pulse for the cross-correlator.

In general, the capability of a pulse shaping tool is given by the theoretically shortest possible temporal pulse distortion which can be introduced by the device (δt) [8]. It is expressed as: $\delta t = T * R/B$, with T and B the pulse duration and spectral bandwidth, respectively, and R the spectral resolution of the shaping device. Calculations indicate that the UV AOPDF is capable to handle temporal features on a time scale of 500 fs for a 2 nm bandwidth input pulse centered at 270 nm which covers well the requirements of our application. In contrast to other schemes [13], the UV AOPDF offers the same temporal pulse complexity for any spectral window between 250 nm and 400 nm without any realignment. Moreover the efficiency of the AOPDF (specified as >20%) is constant over its whole spectral range when operated under the TPA threshold. This is a great advantage when using a wavelength-tunable laser source.

3 Direct shaping of picosecond UV pulses

The combination of UV stretcher and UV AOPDF is a powerful assembly for the generation of complex ps pulse shapes directly in the UV. While the UV stretcher is used to stretch the initial Gaussian pulse from 100 fs to the ps regime, sophisticated amplitude and phase manipulation are performed with the UV AOPDF [24].

To demonstrate the shaping capabilities of our scheme, we recorded a reference temporal profile after the stretcher and UV AOPDF without performing shaping. In this configuration, the AOPDF spectral amplitude filter $F(\omega)$ and spectral phase $\Phi(\omega)$ are set in the AOPDF command software window so that neither spectral amplitude nor phase shaping is applied. More precisely, we set $F(\omega) = \exp(-(\omega - \omega_0)/\delta\omega_0)^6$ at a central wavelength $\lambda_0 = 270.6$ nm and a width $\delta\lambda = 4$ nm in order not to modify the input pulse spectrum (Fig. 2a). $\Phi(\omega)$ is set selecting the so-called *self-compensated mode* in the software command window. This means that the applied spectral phase by the AOPDF exactly compensates the material dispersion of its birefringent crystal. The resulting temporal cross correlation trace is shown in Fig. 2a and the corresponding spectrum in Fig. 2b. The spectrum is centered at 270.6 nm with a spectral width of 1.3 nm FWHM. The unshaped pulse is 5.1 ps long (FWHM) with 2 ps rising and falling edges (10%–90% in intensity) for a prism separation of 1.7 m. The maximum pulse energy is 37 μJ in the diffracted order of the AOPDF for an input energy of 325 μJ.

In order to numerically predict the required UV AOPDF spectral phase and spectral amplitude filtering functions, we performed simulations. From the recorded UV spectrum after the THG stage, the code is calculating the UV pulse temporal profile (via Fourier transform) with a flat spectral phase. The effect of linear propagation of the pulse

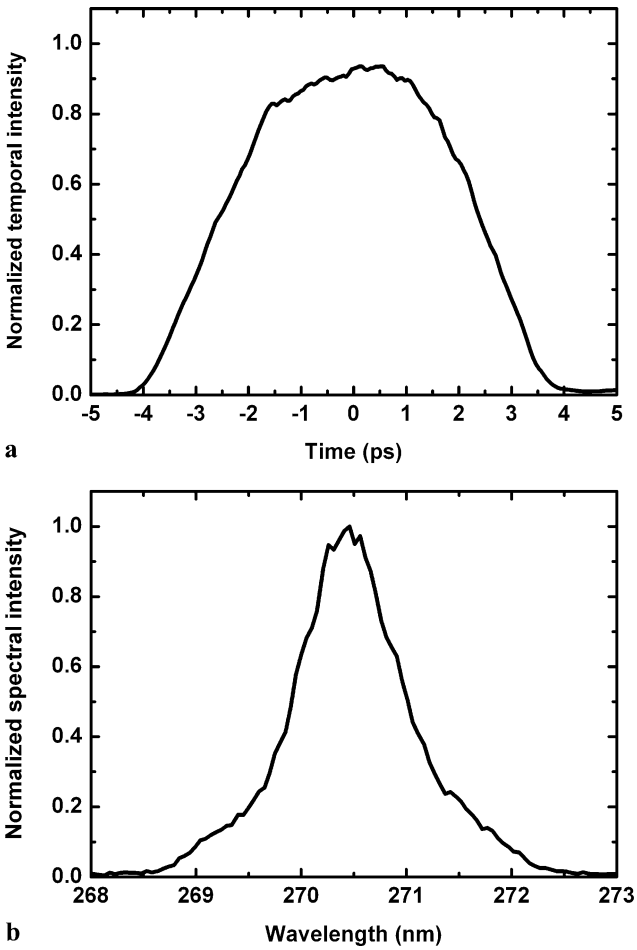

Fig. 2 (**a**) Measured cross correlation temporal intensity profile of the stretched but unshaped 5.1 ps FWHM pulse. The duration of the IR pulse used for the cross correlation is 100 fs FWHM. The measurement is averaged over 8 scans of the cross-correlator. (**b**) Measured spectral intensity of the initial stretched but unshaped pulse (integration time: 30 ms)

through all dispersive elements is computed in the spectral domain. This is done calculating the introduced linear spectral phase contributions of the UV prism stretcher [26], optics [27], and air [28]. The linear spectral amplitude and spectral phase shaping introduced with the UV AOPDF are also taken into account. The shaped UV pulse temporal profile is computed via Fourier transform taking into account the new calculated spectral amplitude and spectral phase. For sake of completeness, we simulated the cross correlation of the UV pulse with the transform-limited IR pulse of 100 fs FWHM used in the experiment. The influence of the nonlinear absorption effect occurring in the UV AOPDF crystal on the final pulse shape is also considered in our calculations. This is done by ponderating the linear intensity profile with the measured intensity dependant transmission of the AOPDF. Calculation of the specific nonlinear absorption coefficient of the UV AOPDF crystal has already been reported elsewhere ($\beta = 2.7$E10 cm/W) [16]. Our simula-

tions indicate that a flattop like temporal pulse profile of an initially Gaussian-like pulse is achieved by mainly introducing fourth-order dispersion (FOD) with the AOPDF. Experimental results confirm this trend and an example is shown in Fig. 3. Applying second- and fourth-order dispersion ($\Phi^2 = -4\text{E}4$ fs^2 and $\Phi^4 = +1\text{E}9$ fs^4) and introducing moderate (15%) amplitude losses at 271 nm the initial 5.1 ps Gaussian pulse (Fig. 2) is reshaped to a 4.6 ps FWHM flat top pulse (Fig. 3a). In order to introduce the desired amount of spectral phase, the width of the AOPDF spectral filter $F(\omega)$ needs to be reduced to $\delta\lambda = 2$ nm. A reduction of the transmitted bandwidth is required to optimize the overlap of the acoustic wave with the optical pulse within the UV AOPDF crystal. To achieve the desired profile, we optimize iteratively spectral amplitude and phase introduced by the UV AOPDF while looking at the cross correlation trace. Such amplitude and phase shaping results in the flattop-like measured temporal pulse shape (black, dotted) with only small amplitude modulations in the plateau region being less than 5% rms. Spectral phase shaping significantly reduces the rising/falling slope of the Gaussian pulse from 2 ps (Fig. 2) to 500 fs (10%–90% in intensity). Figure 3b shows the corresponding measured pulse spectrum (solid line) and the calculated spectral phase (dotted line). Such a high-quality flattop pulse shape is well suited for a laser-driven electron gun where sharp temporal edges and a flat top temporal profile are important demands. The experimental measurements are in well agreement with the numerical expectations (red line). Two numerical parameters differ, however, slightly from the experimental observations. First, the stretcher distance (prism-pair to prism-pair) needs to be systematically reduced in our simulations by 15% to match the measured pulse duration. We attribute this difference to the fact that a point source is assumed at the stretcher entrance. Second our code predicts a ≈15% amplitude overshoot at the pulse edges (Fig. 3a) in contrast to our experiment. The discrepancy is not yet fully understood but may arise from a slightly higher nonlinear absorption in the experiment which is expected to wash out intensity modulations. The rise/fall time as well as the pulse length, however, is well predicted by the code.

In principle, the UV AOPDF gives a large degree of freedom for pulse shaping. In Fig. 4, we successfully generated "M shaped", 4.6 ps FWHM pulses by applying spectral amplitude shaping only. The measured (black dotted) and the simulated (red) temporal cross correlation are displayed in Fig. 4a. The depth and width of the temporal intensity depression can easily be varied by introducing the desired spectral loss in the UV AOPDF spectral amplitude filtering function. Figure 4b shows the corresponding measured pulse spectrum and calculated spectral phase. The spectral phase applied by the UV AOPDF is ($\Phi^2 = -3.5\text{E}4$ fs^2,

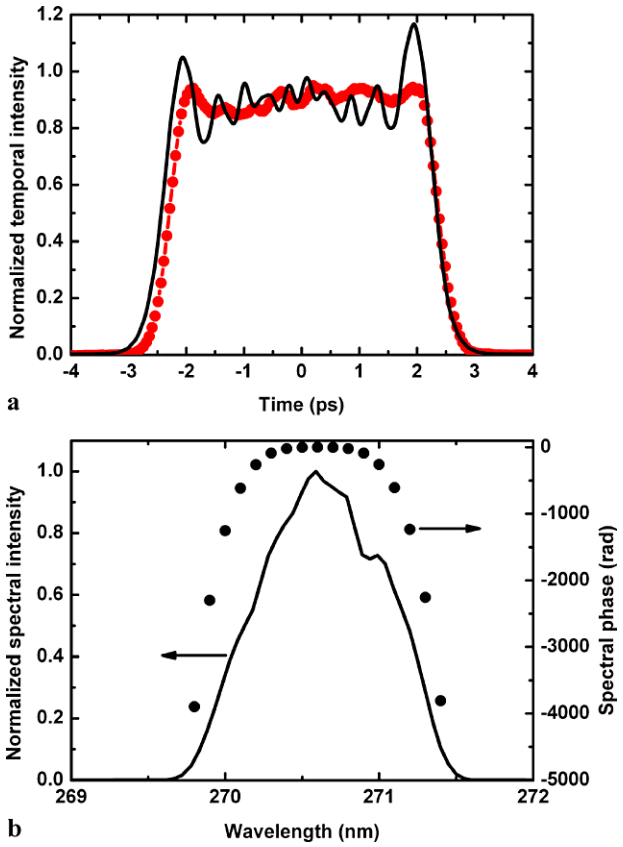

Fig. 3 (**a**) Measured cross correlation temporal intensity profile of a flat top pulse (*red dotted line*). The pulse FWHM duration is 4.6 ps, rise time is less than 0.6 ps (10%–90% in intensity) and the modulation depth on top is <5% RMS. The measurement is averaged over 8 scans of the scanning DFM cross-correlator. The calculated cross correlation trace (assuming a 100 fs IR pulse) is displayed in the *black solid line*. (**b**) Measured spectral intensity of the initial stretched but unshaped pulse (*black solid line*) and calculated spectral phase of the flat top pulse (*black dots*)

$\Phi^3 = -1.5\text{E}6$ fs^3 and $\Phi^4 = 7.8\text{E}4$ fs^4). Due to the dominant linear chirp the temporal pulse shape in Fig. 4a resembles the spectral intensity distribution (Fig. 4b) as expected from theory. Finally, picosecond asymmetrical pulses with a linearly increasing leading edge followed by a fast intensity drop are generated (Fig. 5a). The measured (black) and calculated pulse temporal profile show again an excellent agreement. Figure 5b shows the original spectrum in a green dashed line. Spectral amplitude shaping was performed with the UV AOPDF in order to obtain an asymmetrical spectrum (Fig. 5b black solid line) and by introducing additional second-, third-, and fourth-order dispersion ($\Phi^2 = -5\text{E}4$ fs^2, $\Phi^3 = -4.8\text{E}6$ fs^3 and $\Phi^4 = -9\text{E}8$ fs^4) with the Dazzler to obtain a linearly increasing leading edge. The calculated corresponding spectral phase is also shown in Fig. 5b.

All of the three above presented UV pulses shapes will be used in near future for electron bunch generation on a metal photocathode. Since the electron density is an exact copy

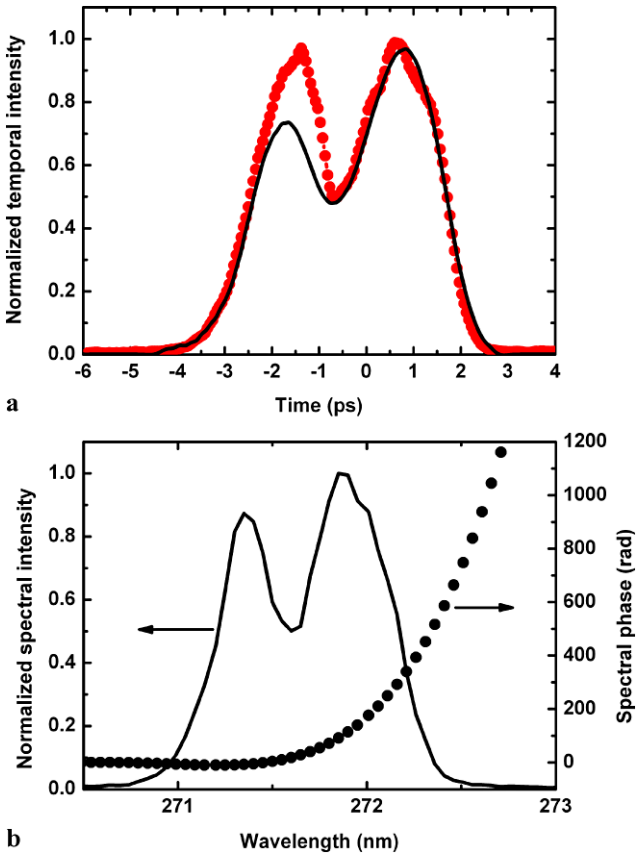

Fig. 4 (**a**) Measured cross correlation temporal intensity profile of the M shaped pulse (*red dotted line*). The *black curve* shows the calculated cross correlation trace (assuming a 100 fs IR pulse). The measurement is averaged over 8 scans. (**b**) Measured spectral intensity of M shaped pulse (*black solid line*) and corresponding calculated spectral phase (*black dots*)

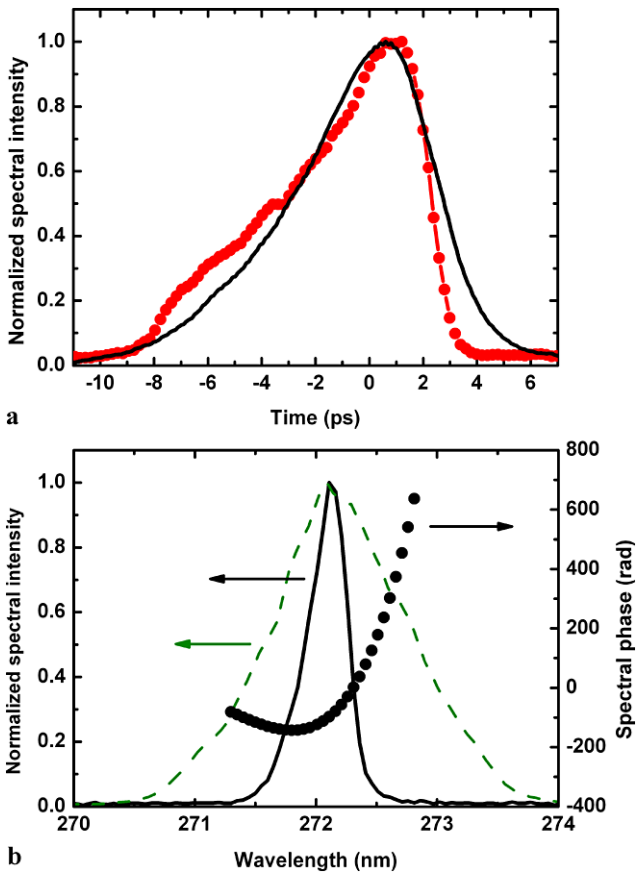

Fig. 5 (**a**) Measured cross correlation temporal intensity profile of the ramp pulse (*red dotted line*). The *black solid curve* shows the calculated cross correlation trace (assuming a 100 fs IR pulse and taking into account nonlinear absorption in the UV AOPDF). The measurement is averaged over 8 scans. (**b**) Measured spectral intensity of the initial pulse (*green dashed line*), of the ramp pulse (*black solid line*) and corresponding calculated spectral phase (*black dots*)

of the UV laser energy, the electron characteristics such as their emittance can be influenced. Systematic studies will be performed after acceleration to 250 MeV to verify the most suitable pulse shape for brightest electron bunch formation. An excellent day-to-day reproducibility of the temporal profiles was observed when the initial laser parameters were kept constant.

4 Spatiotemporal effects

A large beam size (40 mm at $1/e^2$) in the prism stretcher is required to avoid nonlinear absorption. To verify spatial beam quality (e.g., spatial chirp), we recorded spectra across the horizontal transverse beam intensity profile by help of an optical fiber (300 µm core). A measurement of the initial beam prior to the stretcher entrance serves as a reference to quantify the spatial chirp introduced by the stretcher itself. Shown in Fig. 6 are the spectra recorded before (black solid line) and after (red dotted line) the prism stretcher at three different locations across the transverse beam profile (center −1 cm, center, center +1 cm). No significant chirp could be measured (Fig. 6), which is indicated by the excellent overlap of the reference spectra with the spectra recorded at the stretcher exit. We confirm that the UV AOPDF adds some minor additional spatial chirp due to a small wavelength-dependent lateral shift. A detailed study on spatiotemporal effects in the UV AOPDF has been performed elsewhere [23, 29].

5 UV AOPDF efficiency

For high energy applications, the efficiency of the UV AOPDF is of major importance. Figure 7 shows the diffracted energy (blue circles) and the overall transmission (green squares) of the UV AOPDF as a function of the input energy measured for a fixed pulse duration of 5.1 ps FWHM. We observed a nonlinear dependency of the diffracted beam efficiency with increasing input energy. The AOPDF trans-

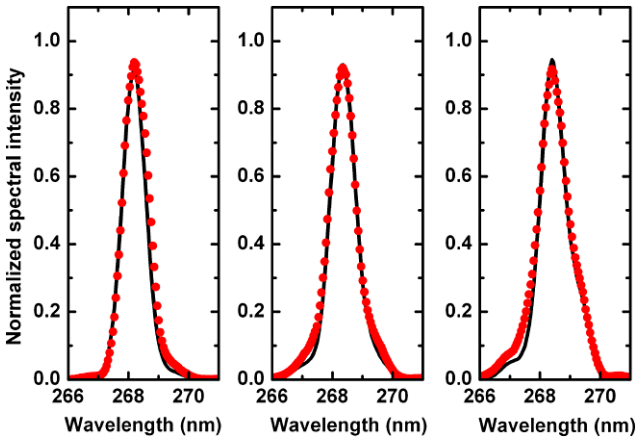

Fig. 6 UV spectra for three different locations across the transverse beam profile (40 mm) along the horizontal axis. *Left*: 1 cm left from the beam centroid, *middle*: centre of the beam (centroid), *right*: 1 cm right from the beam center. Spectra were recorded before (*black solid line*) and after (*red dots*) the prism stretcher

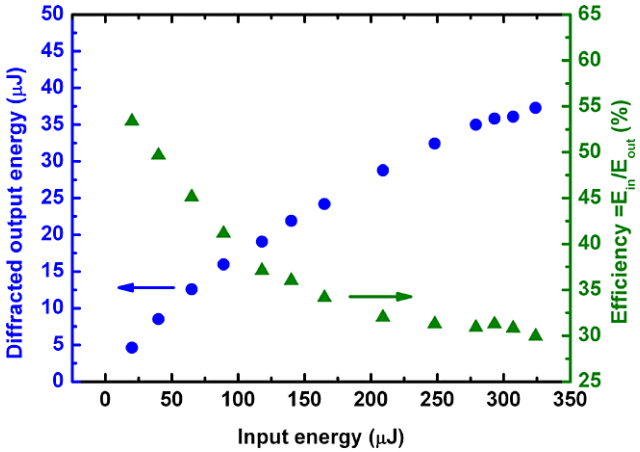

Fig. 7 Measured diffracted output energy (*blue circles*) and overall transmission (*green triangles*) of the AOPDF device as a function of the input energy at 270.6 nm. The pulse duration is set to 5.1 ps FWHM. Two-photon absorption reduces the overall transmission of the device for higher input pulse energies

mission decreases from 54% to 30% for an input pulse energy increased from 20 μJ to 325 μJ. We assign this behavior to two-photon absorption (TPA) in the Potassium dihydrogenphosphate (KDP) crystal of the AOPDF [27]. The efficiency of the UV AOPDF ($E_{\text{diffracted}}/E_{\text{input}}$) is measured to be 23% for low input energy (<20 μJ). At higher input energies (340 μJ) the efficiency dropped to 10.3%.

TPA limited the maximum pulse energy after the AOPDF to 37 μJ (for Gaussian pulse) in the diffracted order. Due to spectral shaping, the maximum energy of the flat top pulse presented in Fig. 4 is measured to be 22 μJ. This is to our knowledge the highest energy ever achieved with this shaping technique. Nonlinear absorption in the UV AOPDF crystal may lead to decreased transmission or damage of the device during continuous long term operation inducing small deviations in the pulse calculated spectral phase and the measured pulse. This effect is difficult to quantify. The robustness of the device still needs to be tested during long term operation. To lower the effect of intensity-dependent TPA, it would in principle be beneficial to increase the pulse duration and the beam size prior to the AOPDF crystal. Unfortunately, this is not feasible in our application since pulse durations of 5–10 ps are required. A reduction of the intensity by increasing the beam size in the AOPDF would lead to strong spatial chirp in the diffracted beam and reduced deflection efficiency due to inhomogeneous and partial overlap with the deflecting acoustic wave.

6 Conclusion

In conclusion, we presented a powerful scheme for pulse forming in the deep UV spectral region and demonstrated amplitude and phase shaping of high energy picosecond pulses at 270 nm. The combination of a highly-efficient double-prism stretcher and an AOPDF applied directly in the UV spectral region enables the generation of high-resolved pulse shapes with flattop, asymmetric and "M shaped" temporal profile at a high energy of up to 37 μJ. The scheme offers a flexible shaper for these durations even though its efficiency is limited by two-photon absorption. The outstanding shaping capabilities both in amplitude and phase at high pulse energies is of particular interest for laser-driven electron guns for FELs and ERLs applications demanding complex temporal pulse shapes in the ps regime.

Acknowledgements We acknowledge funding from the Swiss National Science Foundation under Grant 200021_12211 and Grant PP00P2_128493 (CPH) and are grateful to C. Vicario for fruitful discussions.

References

1. A. Assion, T. Baumert, M. Bergt, T. Brixner, B. Kiefer, V. Seyfried, M. Strehle, G. Gerber, Science **282**, 919 (1998)
2. M. Kotur, T. Weinacht, B.J. Pearson, S. Matsika, J. Chem. Phys. **130**, 134311-5 (2009)
3. A. Monmayrant, B. Chatel, B. Girard, Phys. Rev. Lett. **96**, 103002 (2006)
4. A. Cianchi, Phys. Rev. Spec. Top., Accel. Beams **11**, 032801 (2008)
5. S. Cialdi, M. Petrarca, C. Vicario, Opt. Lett. **31**, 2885 (2006)
6. V. Miltchev, Investigations on the transverse phase space at a photo injector for minimized emittance. Ph.D. Thesis, Berlin University (2006)
7. J. Yang et al., J. Appl. Phys. **92**, 1608 (2002)
8. A.M. Weiner, Rev. Sci. Instrum. **71**, 1929 (2000)
9. T. Tanigawa, Y. Sakakibara, S. Fang, T. Sekikawa, M. Yamashita, Opt. Lett. **34**, 1696 (2009)
10. M. Hacker, T. Feuer, R. Sauerbrey, T. Luzca, G. Szabo, J. Opt. Soc. Am. B **18**, 866 (2001)

11. D.S.N. Parker, A.D.G. Nunn, R.S. Minns, H.H. Fielding, Appl. Phys. B **94**, 181 (2009)
12. P. Nuernberger, G. Vogt, R. Selle, S. Fechner, T. Brixner, G. Gerber, Appl. Phys. B **88**, 519 (2007)
13. B.J. Pearson, T. Weinacht, Opt. Express **15**, 4385 (2007)
14. Y. Oishi, A. Suda, F. Kannari, K. Midorikawa, Opt. Commun. **270**, 305 (2007)
15. http://www.brimrose.com/pdfandwordfiles/aomodu.pdf
16. A. Dragonmir et al., Appl. Opt. **41**, 4365 (2002)
17. A. Dubietis, G. Tamosauskas, A. Varanavicius, G. Valiulis, Appl. Opt. **39**, 2437 (2000)
18. M. Hacker, G. Stobrawa, R. Sauerbrey, T. Buckup, M. Motzkus, M. Wildenhain, A. Gehner, Appl. Phys. B **76**, 711 (2003)
19. S.M. Weber, J. Extermann, L. Bonacina, W. Noell, D. Kiselev, S. Waldis, N.F. de Rooij, J.P. Wolf, Opt. Lett. **35**, 3102 (2010)
20. A. Rondi, J. Extermann, L. Bonacina, S.M. Weber, J.P. Wolf, Appl. Phys. B **96**, 757 (2009)
21. J. Mohring, T. Buckup, M. Motzkus, Opt. Lett. **35**, 3916 (2010)
22. S. Weber, M. Barthelemy, B. Chatel, Appl. Phys. B **98**, 323 (2010)
23. N. Krebs, R.A. Probst, E. Riedle, Opt. Express **18**, 6164 (2010)
24. S. Coudreau, D. Kaplan, P. Tournois, Opt. Lett. **31**, 1899 (2006)
25. A.A. Fotiadi, G. Brambilla, T. Ernst, S.A. Slattery, D.N. Nikogosyan, J. Opt. Soc. Am. B **24**, 1475 (2006)
26. Z. Cheng, F. Krausz, Ch. Spielmann, Opt. Commun. **201**, 145 (2002)
27. www.corning.com/docs/specialtymaterials/pisheets/H0607_hpfs_Standard_ProductSheet.pdf
28. E.R. Peck, K. Reeder, J. Opt. Soc. Am. **62**, 958 (1972)
29. D.J. McCabe, D.R. Austin, A. Tajalli, S. Weber, I.A. Walmsley, B. Châtel, J. Opt. Soc. Am. B **28**, 58 (2011)